available at www.sciencedirect.com

ScienceDirect

journal homepage: www.elsevier.com/locate/jmbbm

Research paper

Tribo-mechanical characterization of rough, porous and bioactive Ti anodic layers

Gelson B. de Souza[a,*], *Gabriel G. de Lima*[b], *Neide K. Kuromoto*[b], *Paulo Soares*[c],
Carlos M. Lepienski[b], *Carlos E. Foerster*[d], *Alexandre Mikowski*[b,e]

[a] *Sciences Department, Universidade Estadual de Maringá, 87020-900, Maringá, PR, Brazil*
[b] *Physics Department, Universidade Federal do Paraná, 81531-990, Curitiba, PR, Brazil*
[c] *Mechanical Engineering Department, Pontifícia Universidade Católica do Paraná, 80215-901, Curitiba, PR, Brazil*
[d] *Physics Department, Universidade Estadual de Ponta Grossa, 84030-900, Ponta Grossa, PR, Brazil*
[e] *Mobility Engineering Center, Universidade Federal de Santa Catarina, 89219-905, Joinville, SC, Brazil*

ARTICLE INFO

ABSTRACT

Rough and porous titanium oxide layers, which are important features for improving the osseointegration of Ti implants with bone tissues, are obtained through the technique of anodic oxidation. The thicknesses of such coatings are typically in the order of micrometers, and their mechanical characterization can be assessed by instrumented indentation, provided that the composite nature of the surface is considered. Titania anodic layers were produced on Ti under galvanostatic mode using Ca–P-based electrolytes (a mixture of $(CH_3COO)_2Ca \cdot H_2O$ and $NaH_2PO_4 \cdot 2H_2O$), employing current densities (J) of 150 mA/cm^2 and 300 mA/cm^2. The structure and morphology were characterized by X-ray diffraction (XRD), scanning electron microscopy with electron dispersive X-ray spectroscopy (SEM/EDS), and profilometry, and the chemical features were characterized by X-ray photoelectron spectroscopy (XPS). TiO_2 layers presented the crystalline phases rutile and anatase, and incorporation of Ca and P presented as a calcium phosphate compound. The porosity, roughness, and thickness increased with J. Analytical methods were employed to obtain the modified layers' elastic modulus and hardness from instrumented indentation data, deducting the substrate and roughness effects. The elastic moduli were about 40 GPa for both values of J, which are similar to the values for human bones (10–40 GPa). The hardness decreased with indentation load, varying from 5 GPa at the near surface to 1 GPa at the layer–substrate interface. Such hardness behavior is a consequence of the surface brittleness under normal loading. Additional scratch tests using an acute tip indicated that the layer integrity under shear forces was 220 mN ($J = 150$ mA/cm^2) and 280 mN ($J = 300$ mA/cm^2). TiO_2 layers produced with both current densities presented good results for *in vitro* bioactivity tests using simulated body fluid (SBF) solution, which can be attributed to a combined effect of the microstructure, layer porosity, and hydroxyl radicals in plenty at the near surface.

© 2010 Elsevier Ltd. All rights reserved.

1.　Introduction

Among several methods that have been studied to improve titanium osseointegration with living tissues (Chu et al., 2002; de Jonge et al., 2008; Liu et al., 2004), the production of titania coatings by anodic oxidation processes offers some interesting features. Porous layers can be produced using different electrolytes, such as H_2SO_4, H_3PO_4 and Ca–P-based solutions, and setting up the oxidation parameters (voltage, current density, and time) to allow the dielectric rupture of the layer (Sul et al., 2002). Besides the improved adhesion with the substrate, the porous structure of such anodic oxide layers favours cell adhesion, and, in the presence of body fluids, nucleates hydroxyapatite on their surfaces (Fini et al., 1999; Frauchiger et al., 2004; Kuromoto et al., 2007; Li et al., 2004; Liu et al., 2004; Yang et al., 2004; Zhu et al., 2001). The hydroxyapatite nucleated on the biomaterial surface can work as the means to a direct implant–bone connection, without intermediate fibrous tissues, as verified by Nishiguchi et al. (1999, 2001) using *in vivo* tests. According to the literature, these conditions promote a better fixation strength, which can be achieved in earlier periods of *in vivo* implantation (Liu et al., 2004; Nishiguchi et al., 1999, 2001; Paital and Dahotre, 2009). The hydroxyapatite nucleation is mostly attributed to the large number of hydroxyl radicals at the oxide layer, produced during the dielectric rupture regime, which triggers interactions between calcium and phosphates from the body fluid with the surface (Liu et al., 2004; Chen et al., 2006).

In addition to the osseointegration capability, the mechanical properties of anodic layers are also important features to ensure long implant lifetime (Liu et al., 2004; Mändl and Rauschenbach, 2002). The recovery of a bone that has been damaged by fracture or surgical processes is influenced by the mechanical stress on it. Stress shielding, i.e., the reduction or absence of mechanical stress in the bone, causes atrophy or absorption of the bone tissue. Such a detrimental effect can also occur in artificial prosthesis, even if the implant site is under regular loading conditions by the patient. In this situation, stress shielding is due to large differences between the elastic moduli of the bones and the implant, which make the load transfer from the body to the prosthesis difficult. A reduction in the mechanical stresses occurs around the implant, inducing bone resorption, osseous atrophy, and even prosthesis release (Niinomi et al., 2004). Among the metals used as biomaterials, titanium and its alloys (such as Ti–6Al–4V) present the lowest elastic modulus (~100 GPa), which is considered a biomechanical benefit to prevent stress shielding (Liu et al., 2004; Niinomi, 2008). However, this elastic modulus is still five times larger than that of cortical human bone (~20 GPa). Studies have been conducted in order to obtain novel Ti alloys with stiffness closer to that of bone tissues (Niinomi, 2003). On the other hand, the load transference can be improved by tailoring the implant surface properties, since mechanical interactions are critical at the interface between artificial material and living tissues.

Instrumented indentation is an appropriate method to mechanically characterize thin coatings and modified surfaces (Oliver and Pharr, 2004), and it has been used in the study of bioactive layers (Santos Jr. et al., 2007; Soares et al., 2008). However, the determination of the elastic modulus (*E*) and hardness (*H*) of the porous anodic layers is not simple. Substrate effects influence the values measured by instrumented indentation (Saha and Nix, 2002), and roughness and porosity cause inaccuracies in the *E* and *H* profiles (de Souza et al., 2010a).

Another situation concerning the implant surfaces also demands special attention. During fixation or normal use, the implants are submitted to wear mechanisms by shear forces. There is a (small) chance that the released ionic Ti will combine with biomolecules to cause cytotoxicity, allergy, and other biological influences (Hanawa, 2004). Notwithstanding, the detachment of coatings and debris generation are highly undesirable, since fragments can cause reactions and the necessity of prosthesis replacement (Korkusuz and Korkusuz, 2004).

In this work, commercially pure Ti was anodically oxidized using Ca- and P-based electrolytes. The surface morphology, structural, and chemical features were evaluated, as well as the *in vitro* bioactivity. The layers' tribo-mechanical behavior was studied by using an instrumented indentation device. Analytical methods were employed to obtain the elastic modulus and hardness of the modified layers from indentation data, by taking into account the substrate and roughness effects on the measured values.

2.　Materials and methods

Mechanical characterization at the nanoscale (elastic modulus and hardness calculated from the instrumented indentation data) is strongly affected by the presence of asperities (de Souza et al., 2006, 2010a). Therefore, in order to minimize the roughness effects on the mechanical property results, the Ti samples were prepared to a mirror-like finish, thereby limiting the surface texture to the one produced by the anodic oxidation process. Commercially pure titanium (grade 2) samples were grounded using #600 SiC paper, followed by polishing with 9 μm diamond paste and colloidal silica suspension.

The plates were successively washed with acetone, isopropyl alcohol, and distilled water in an ultrasonic cleaner. Samples were then galvanostatically anodized at room temperature in an electrolytic solution containing 0.14 mol/l calcium acetate monohydrate ($(CH_3COO)_2Ca \cdot H_2O$) and 0.06 mol/l sodium biphosphate dihydrate ($NaH_2PO_4 \cdot 2H_2O$) in deionized water. Two different current densities were applied for 100 s: 150 and 300 mA/cm^2. From this point on, the samples will be denominated by their respective current densities.

The morphology of the layers was analyzed using scanning electron microscopy (SEM) with electron dispersive X-ray spectroscopy (EDS). Structural changes were characterized by X-ray diffraction (XRD) in θ–2θ geometry, using Cu Kα radiation and scan velocity 0.24°/min. The diffraction peaks were indexed using the Inorganic Crystal Structure Database (FIZ, 2008). The average roughness (R_a) and layer thickness were determined using a stylus profilometer. The surface profile was integrated by the ensemble of 2000 data points assembled across the scan length of 1000 μm, in ten different surface sites. The value of R_a was calculated according to the literature (Bhushan, 2001).

The chemical nature of the untreated Ti and modified surfaces was investigated by X-ray photoelectron spectroscopy (XPS), performed using VG Microtech ESCA 3000 equipment with a 3×10^{-8} Pa vacuum. Al Kα radiation and band-pass energies of 50 and 20 eV were used for the survey and high-resolution measurements, respectively. The overall resolution was 0.8 eV. The binding energy of elemental peaks was corrected with reference to the C 1s signal at a standard binding energy of 284.5 eV. For background subtraction, the Shirley method (Moulder et al., 1992) was used, and deconvolution of peaks was done using Fityk® software (Wojdyr, 2010).

The untreated and anodic oxidized samples were soaked in a simulated body fluid (SBF) at 36.5 °C for 14 days to verify the surface bioactivity. The SBF was prepared according to the Kokubo and Takadama (2006) recipe.

The elastic modulus and hardness were evaluated by instrumented indentation following the Oliver and Pharr (2004) method with a diamond Berkovich tip. Seven complete load–unload cycles with loads ranging from 4.7 to 300 mN were carried out. Each sample was indented in 85 different sites. The effective elastic modulus and hardness of the layers, discounting the effects of the substrate, were calculated by the Xu and Pharr (2006) and Bhattacharya and Nix (1988) analytical methods, respectively. Nanoscratch tests were carried out with the Berkovich tip by the same instrumented indentation device. The linear ramping loads start at 0.03 mN, reaching 400 mN, after 600 µm, following the tip edge direction. The tip penetration profiles were monitored before, during, and after the scratch. The profiles during the loading and the elastic recovery were determined, taking into account the original surface topography.

3. Results

3.1. Structural features, morphology and bioactivity

Fig. 1(a)–(b) present the X-ray spectra for untreated Ti and samples oxidized using the two applied current densities (150 and 300 mA/cm^2). In Fig. 1(a), the TiO$_2$ phases rutile (R) and anatase (A) were identified for both current densities. The rutile phase was more evident in the 300 mA/cm^2 sample, whereas anatase peaks predominated in the 150 mA/cm^2 sample. Otherwise, oxide peaks are more intense in the 300 mA/cm^2 sample than in the 150 mA/cm^2 sample, possibly indicating that these elements are more abundant in higher current density conditions. It is reported that anodizations performed in Ca and P solutions present these elements in the layer, possibly forming amorphous compounds (Li et al., 2004; Liu et al., 2005; Yu et al., 2007). Chen et al. (2006) reported that crystalline hydroxyapatite (HA) was identified in the layers produced with Ca and P solutions. Indeed, in Fig. 1(a), both samples present a reflection at $\sim 31.7°$, more intense in the 300 mA/cm^2 sample, which can be attributed to calcium phosphate phases. Several calcium phosphates share X-ray diffraction peaks in similar positions, for the same radiation (FIZ, 2008). In Fig. 1(a) the proper position of the calcium phosphate peak is difficult to define due to its low intensity; however, it is indexed as
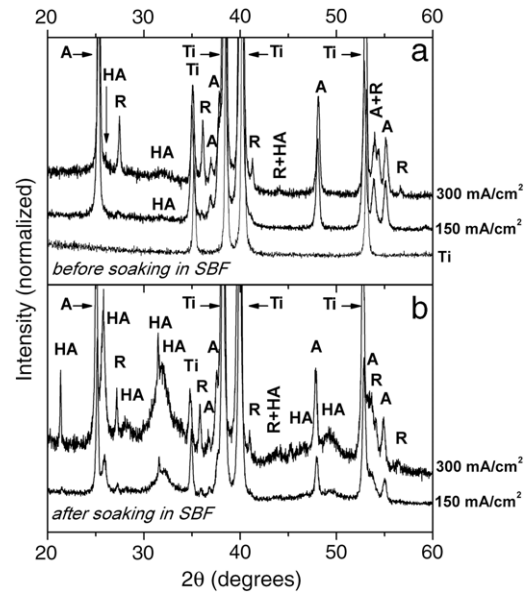

Fig. 1 – (a) X-ray diffractograms for untreated Ti and the samples anodically oxidized using current densities of 150 and 300 mA/cm^2. The peak at ~31.7° is attributed to a calcium phosphate phase. In (b) X-ray diffractogram for the oxidized samples after soaking in SBF for 14 days.
A = anatase; R = rutile; HA = hydroxyapatite.

hydroxyapatite (HA) in accordance with the Chen et al. (2006) work.

After the SBF soaking periods, no differences were observed in the untreated Ti. In the oxidized samples, as shown in Fig. 1(b), XRD analysis revealed diffraction peaks corresponding to the "new" hydroxyapatite produced, overlapping the previous calcium phosphate peaks, in addition to other HA reflections. The peak situated at $2\theta \sim 31.5°$ (the main HA reflection, FIZ, 2008) is quite narrow for both samples, indicating that the hydroxyapatite produced in SBF presents a high degree of crystallinity.

At a first microscopic observation, after the anodic oxidation process, the surface of the metallic titanium that was in contact with the electrolyte presented a gray color, and this became whiter with increase of the current density. The layers are porous and present similar morphologies, as indicated in the SEM micrographs of Fig. 2(a)–(b). Pores are produced in the dielectric rupture regime due to the spark production and H$_2$ and O$_2$ release at the electrolyte–substrate interface. The pore size increases with the current density, from an average diameter of 0.9 µm (150 mA/cm^2) to 3 µm (300 mA/cm^2). Likewise, the average roughness (R_a) and layer thickness, determined by profilometry, also seem to be current density dependent; the results are summarized in Table 1. Cracks were observed in all the layer area, for both samples, as indicated in the insets of Fig. 2(a)–(b). EDS results (Fig. 2(c)) show the presence of Ca and P elements before soaking in SBF, in both 150 mA/cm^2 and 300 mA/cm^2 samples, corroborating the XRD results of Fig. 1(a). The Ca/P ratios determined by EDS analysis were (1.05 ± 0.06) and (1.09 ± 0.07) for the 150 and 300 mA/cm^2 samples, respectively. Moreover, according to Zhu et al. (2001), the Ca

Table 1 – Thickness, average roughness, elastic modulus, hardness, and critical load for scratch tests of Ti samples submitted to anodic oxidation using the indicated current densities.

Current density	Film thickness (μm)	Average roughness (μm)	Elastic modulus (GPa)	Hardness (GPa)	Critical load for scratch tests (mN)
0 (untreated)	–	–	135 ± 4	2.7 ± 0.2	–
150 mA/cm^2	3.6 ± 0.3	0.37 ± 0.05	46 ± 11[a]	1.7 ± 0.5[b]	220 ± 10
300 mA/cm^2	4.1 ± 0.5	0.82 ± 0.20	36 ± 16[a]	1.5 ± 0.6[b]	280 ± 20

[a]Values obtained at 1.5 μm in depth from Fig. 5, and subtracting the substrate effects (see Section 3.3).
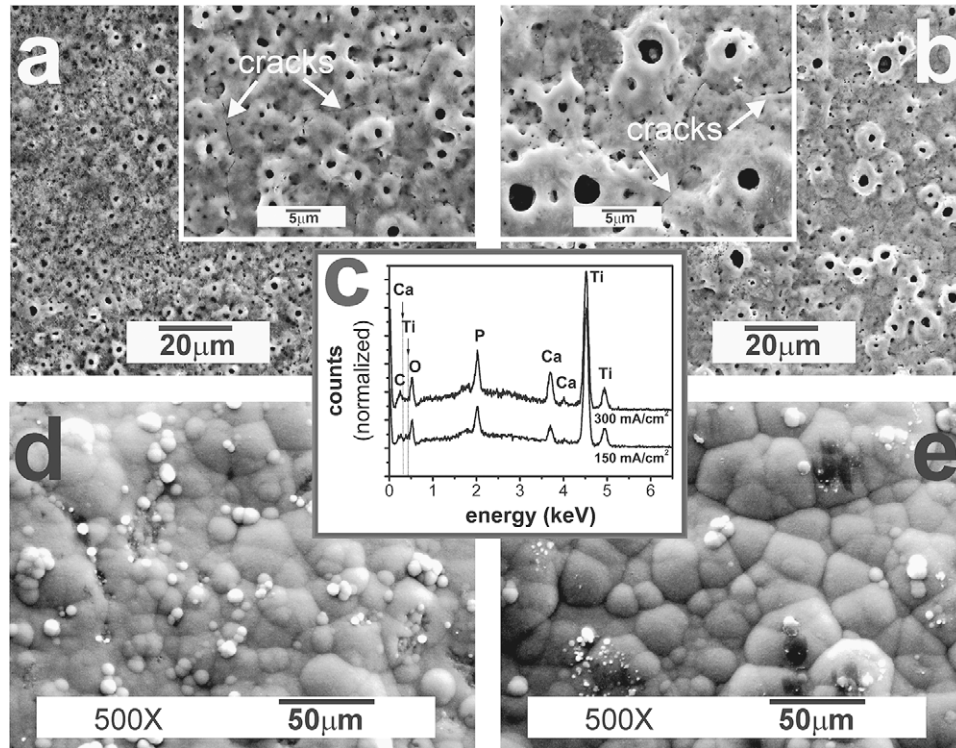[b]Values obtained at 1.5 μm in depth from Fig. 6, and subtracting the substrate effects (see Section 3.4).

Fig. 2 – SEM micrographs of samples anodically oxidized using current densities of (a) 150 mA/cm^2 **and (b)** 300 mA/cm^2. **In the insets, it can be observed that there are cracks on the layer surfaces, and also that the pore size increases with the current density. (c) EDS spectra for both produced layers. After soaking in SBF for 14 days, hydroxyapatite nucleated on both (d)** 150 mA/cm^2 **and (e)** 300 mA/cm^2 **samples.**

content increase with the current density (Fig. 2(c)) can be related to the observed sample brightening.

After soaking samples in SBF for 14 days, as shown in Fig. 2(d)–(e), new layers were observed on the anodized samples, which, as verified by XRD (Fig. 1(b)), correspond to nucleated hydroxyapatite. However, no nucleation was observed in the untreated Ti. The hydroxyapatite layers present similar morphologies for both 150 and 300 mA/cm^2 samples.

3.2. Chemical features

The anodic layers produced on Ti were investigated by XPS in order to analyze the chemical nature of the elements at the near surface. Fig. 3(a) shows the survey spectra for the reference Ti sample, and for the 150 and 300 mA/cm^2 samples. The reference surface presented peaks at binding energies corresponding to titanium, oxygen (from the oxide native layer),

and carbon (possibly from surface contaminants). The relative intensity of the oxygen increases after anodization for both current densities. In addition, calcium and phosphorus peaks appear at the anodic layer, in accordance with EDS and XRD results, and also with several authors who performed anodic oxidations using Ca–P-based solutions (Chen et al., 2006; Fini et al., 1999; Li et al., 2004; Liu et al., 2005; Yu et al., 2007; Zhu et al., 2001).

Elemental high-resolution analyses were performed for the Ti 2p, O 1s, Ca 2p and P 2p binding energies. The Ti 2p doublet spectra were similar for all the conditions studied (reference Ti, and 150 and 300 mA/cm^2 samples), presenting peaks centered at 458.5 eV (Ti 2p$_{3/2}$) and 464.3 eV (Ti 2p$_{1/2}$). These binding energies are assigned to the Ti–O bonds in TiO$_2$ (Battistoni et al., 2000; Combes et al., 1998; NIST, 2010). The TiO$_2$ on the reference sample can be attributed to the native oxide layer, whose thickness is typically 2–5 nm (Yen, 1999).
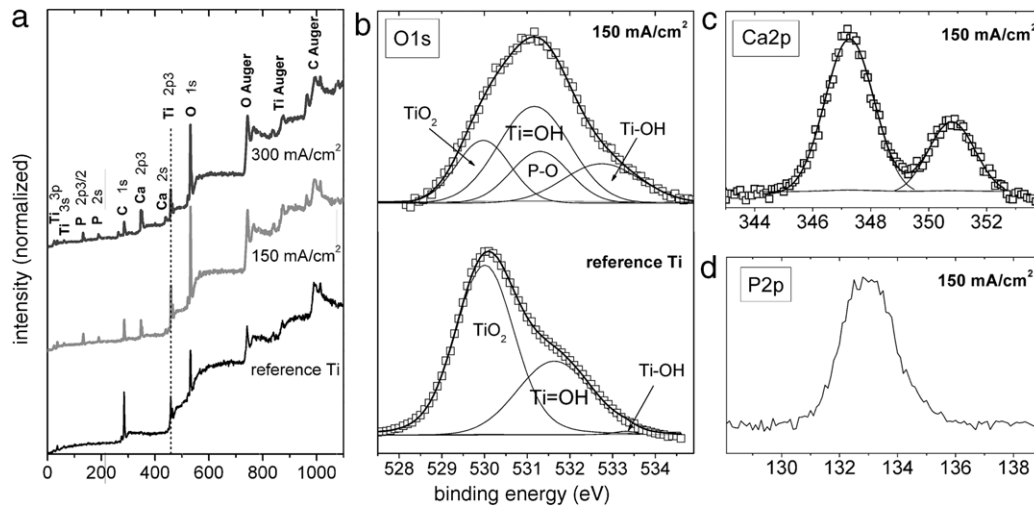
Fig. 3 – XPS spectra obtained on the reference Ti sample and samples anodically oxidized with Ca- and P-based electrolytes using the current densities 150 and 300 mA/cm^2: **(a) survey; (b) O 1s; (c) Ca 2p; (d) P 2p.**

The two anodization conditions also presented similar O 1s, Ca 2p and P 2p spectra, pertaining to the peak shapes and energy ranges, and are represented in Fig. 3(b)–(d) by the 150 mA/cm^2 sample. The O 1s peak is presented in Fig. 3(b) for the reference and the anodized conditions. In the reference Ti case, it can be deconvoluted into three contributions, in agreement with the literature (Bertóti et al., 1995; Combes et al., 1998; Kunze et al., 2008; Lu et al., 2000; NIST, 2010): TiO$_2$ at 529.9 eV (main contribution, 66%); physically adsorbed water Ti = OH at ~531.5 eV; and chemically adsorbed water Ti–OH at ~533.3 eV. In the anodized surface, the O 1s spectra is shifted to higher binding energies, indicating that the oxygen bonds can be present in compounds other than TiO$_2$. Such oxygen bindings can be attributed to the hydroxyl groups (Ti = OH and Ti–OH) and/or phosphates, as indicated by the peak deconvolution. The P–O bonds in the O 1s spectrum have binding energies around 531.4 eV (Battistoni et al., 2000; de Sena et al., 2003; Kunze et al., 2008; NIST, 2010; Takadama et al., 2001).

The assumption that P–O species can exist at the anodized Ti surface even before the soaking in SBF is corroborated by the analysis of calcium and phosphorus chemical states. The Ca 2p doublet (Fig. 3(c)) has peaks centered at 347.3 eV (Ca 2p$_{3/2}$) and 350.8 eV (Ca 2p$_{1/2}$), which can be assigned to Ca in calcium phosphate molecules (NIST, 2010). Likewise, the P 2p peak (Fig. 3(d)) is centered at 132.9 eV, also typical for P in calcium phosphates (NIST, 2010). Depending on the calcium phosphate stoichiometry, and besides the doublet separation (~0.8 eV), the P 2p peak may present more than a single contribution, since P in phosphates can be linked solely with O and simultaneously with O and H, the last through the oxygen atom (Battistoni et al., 2000; Combes et al., 1998; de Sena et al., 2003; Kunze et al., 2008). However, as mentioned in Section 3.1, the calcium phosphate stoichiometry in the anodic layers could not be clearly determined by XRD. According to data from the literature (Battistoni et al., 2000; Combes et al., 1998; de Sena et al., 2003; Kunze et al., 2008; NIST, 2010; Takadama et al., 2001), the Ca 2p and P 2p binding energies for hydroxyapatite are rather different than the

present ones (Ca2p$_{3/2}$ = 347.8 eV; P 2p = 133.8 eV), which suggests a diverse stoichiometry for the calcium phosphate composing the anodic layers.

3.3. Elastic modulus

Fig. 4 shows three indentation imprints produced on the 300 mA/cm^2 sample with a pyramidal Berkovich tip under 300 mN applied load. Cracks were identified around imprints, as shown in the inset of Fig. 4. This result indicates that the oxide layers are brittle. Besides, the surface topography may also be taken into consideration. When the indentation tip penetration is carried out on a rough surface, the tip interaction with the asperities can lead to errors in the "zero" depth determination in the load versus displacement curves. This alters the maximum penetration value used in the calculation of the elastic modulus and hardness by the Oliver and Pharr (2004) method. The instrumented indentation loading–unloading curves were corrected using the contact stiffness analysis (de Souza et al., 2006, 2010a). According to this method, the correct "zero" depth is obtained by analysis of the load over displacement ratio. The mechanical properties were then recalculated by the Oliver and Pharr method (2004) using the corrected data.

Fig. 5 presents elastic modulus profiles for the untreated Ti, the composite layer plus substrate and the layer values calculated from the composite curve. There are no significant differences between the 150 and 300 mA/cm^2 composites. The elastic moduli at near surface are around 70 GPa, dropping to about 50 GPa up to 500 nm and then increasing toward substrate values (135 GPa) in depths close to the layer–substrate interface (see layer thicknesses in Table 1), but not reaching the substrate value.

The elastic modulus of the layer, subtracting the effects of the Ti substrate, was calculated by means of the analytical method proposed by Xu and Pharr (2006), which extends the Gao et al. proposal (1992) for a widest range of situations. The method demands specific information about the layer and the substrate: layer thickness, substrate elastic modulus,
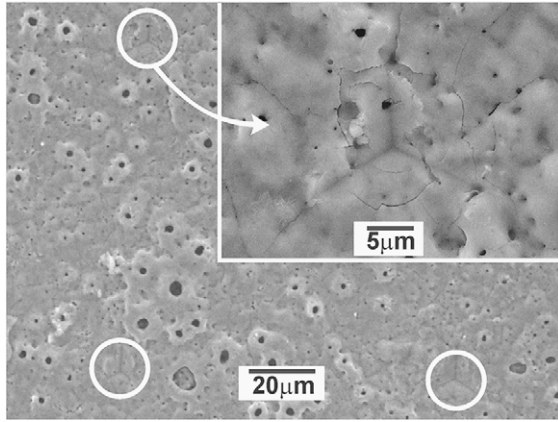
Fig. 4 – The layer produced with 300 mA/cm^2 current density, indicating (circles) three indentation imprints produced with a pyramidal Berkovich diamond tip under 300 mN applied load. The inset shows cracks produced around indentations.
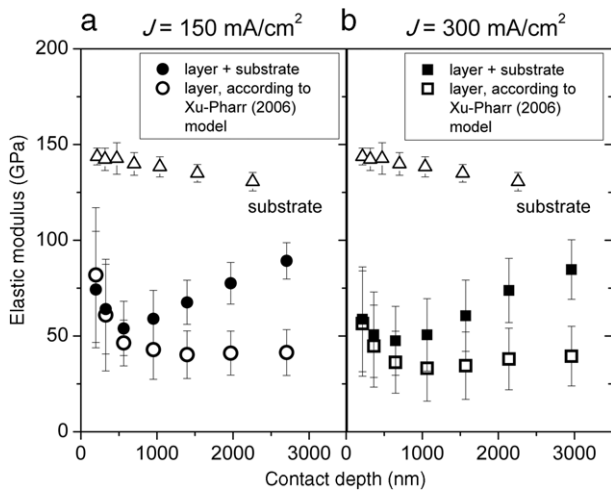

Fig. 5 – Elastic modulus profiles for the untreated sample (substrate) and the Ti submitted to anodic oxidation using current densities of (a) 150 mA/cm^2 and (b) 300 mA/cm^2. The profiles corresponding to the layers, without the substrate effects, were calculated by the Xu and Pharr (2006) analytical method.

and the respective Poisson's ratios. The first two properties are summarized in Table 1. The Poisson's ratio for Ti is well known ($\nu = 0.32$). For the titania layers it was assumed that $\nu = 0.28$ (Soares et al., 2008). Calculations were performed for all points constituting the composite profiles, since they lay inside the layer region (depths up to 3 μm). The calculated values for elastic moduli obtained by the Xu and Pharr model are also presented in Fig. 5. The layer values follow the composite profile up to 300 nm, and from this depth on are approximately constant, around 40 GPa. The corrected values obtained at a penetration depth of 1500 nm (middle region) are summarized in Table 1.
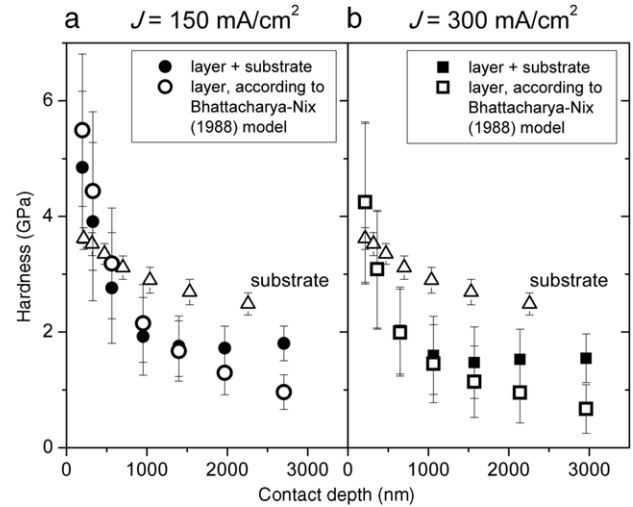

Fig. 6 – Hardness profiles for the untreated sample (substrate) and the Ti submitted to anodic oxidation using current densities of (a) 150 mA/cm^2 and (b) 300 mA/cm^2. The profiles corresponding to the layers, without the substrate effects, were calculated by the Bhattacharya and Nix (1988) analytical method.

3.4. Hardness

The hardness profiles for the composites layer plus substrate, presented in Fig. 6, are similar for the two current densities used, 150 and 300 mA/cm^2. Also, as observed for the elastic modulus, the hardness profiles drop at the near surface, but here diminishing from values above the substrate (~5 GPa) at the near surface to ~1.5 GPa in 3000 nm depth.

The hardness (H) of the layers, subtracting the effects of the Ti substrate, can be calculated by the Bhattacharya and Nix analytical model (1988), given by

$$H_c = H_s + \left(H_f - H_s\right) \exp\left[-\frac{H_f}{H_s} \frac{Y_s}{Y_f} \sqrt{\frac{E_s}{E_f}} \frac{h}{t} \right],$$ (1)

where E is the elastic modulus, Y the yield strength, h the contact depth, and t the layer thickness. The index f indicates the layer and s indicates the substrate. The above equation is valid for the situation where the layer is harder than the substrate, which is applicable in anodic layers (Santos Jr. et al., 2007; Soares et al., 2008). The Bhattacharya and Nix model has been presented as a satisfactory choice to obtain the layer hardness (Fischer-Cripps, 2004). The substrate hardness, layer thickness, and layer and substrate elastic moduli, necessary for calculation by Eq. (1), are presented in Table 1. The yield strength is usually determined by its linear relationship with the hardness, $H = 2.8Y$ (Fischer-Cripps, 2004), so it can be easily calculated for the Ti substrate. Since the layer hardness is the concern of this study, a different approach is needed for the layer yield strength Y_f. Soares et al. (2008) presented a methodology for Y_f calculation, as follows. The titania layer can be considered as a ceramic layer, and its Y_f value can be obtained by the relationship presented by Milman and Chugunova (1999):

$$Y_f = \frac{H_f}{\alpha} \delta_H + \frac{H_f}{\beta} \left(1 - \delta_H\right),$$ (2)
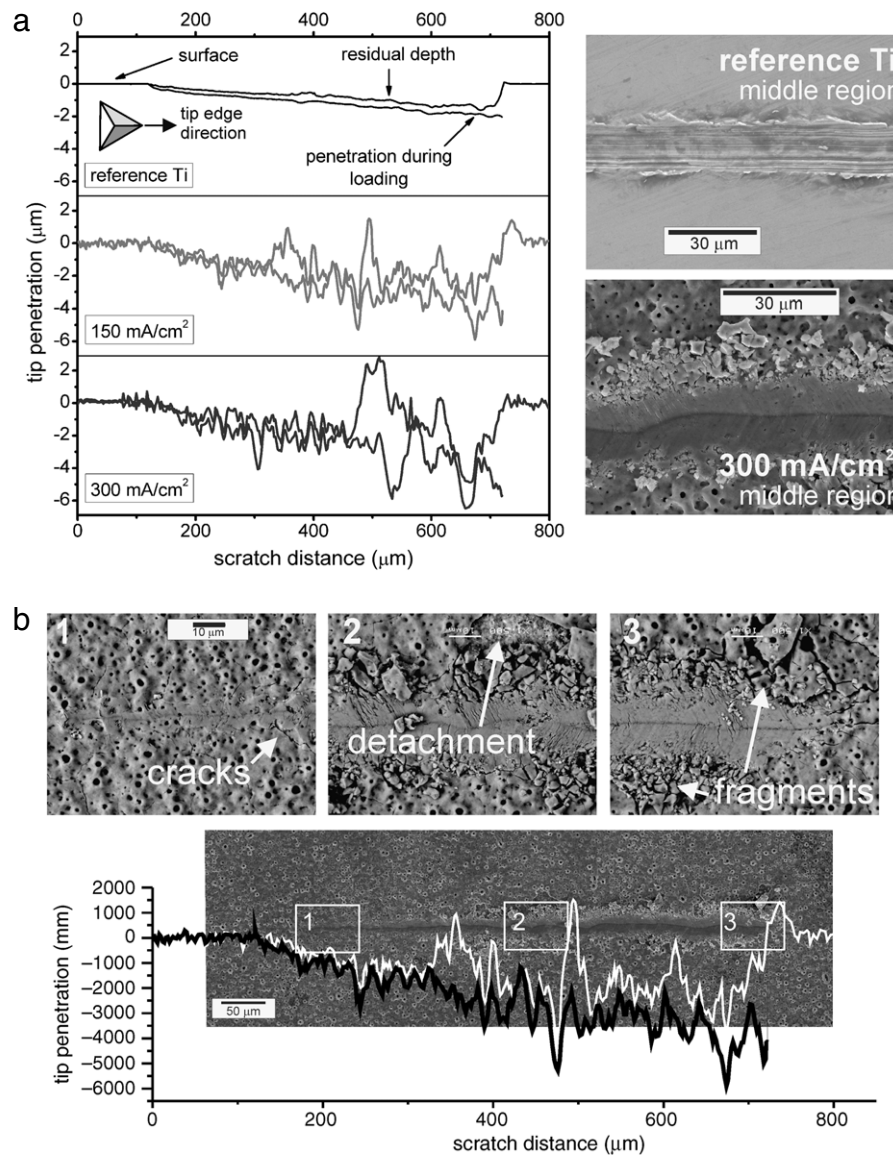
Fig. 7 – Scratch tests performed on the reference Ti sample and samples anodically oxidized with Ca- and P-based electrolytes. (a) Penetration profiles; the SEM micrographs correspond to the grooves middle region (corresponding to the scratching load 200 mN) to the reference and $300\ \mathrm{mA/cm^2}$ samples; (b) the SEM micrograph with the overlapped penetration profile for the $150\ \mathrm{mA/cm^2}$ sample; the insets indicate crack formation, fragment release, and detachment due to surface scratching.

where $\alpha = 4.9$ and $\beta = 2.1$ are numeric parameters and δ_H denotes the material's plasticity. The latter can be obtained using the elastic (ε_e) and total (ε_t) surface deformations from the loading–unloading curves of instrumented indentation tests, by $\delta_H = 1 - (\varepsilon_e/\varepsilon_t)$. This gave $\delta_H = 0.43 \pm 0.18$ for the $150\ \mathrm{mA/cm^2}$ sample and $\delta_H = 0.42 \pm 0.16$ for the $300\ \mathrm{mA/cm^2}$ sample. Thereby, Eq. (2) was combined with Eq. (1) to obtain a relationship for the H_f calculation.

Fig. 6 also presents the layer hardness profiles calculated by the Bhattacharya and Nix model. All values are for inside the layer, that is, above the interface with the substrate. The calculated profiles are very similar to the composite one, presenting no significant differences up to about 2 μm depth ($150\ \mathrm{mA/cm^2}$ sample) and 1.6 μm depth ($300\ \mathrm{mA/cm^2}$).

Values obtained at 1500 nm (middle region) are summarized in Table 1.

3.5. Scratch tests

Scratch tests performed on the treated Ti followed the Berkovich tip edge direction, as illustrated in the inset of Fig. 7(a), which, in a certain manner, simulates the surface sliding against asperities or screw throats. The curves in Fig. 7(a) correspond to the penetration profiles obtained during and after scratching, the last one corresponding to the residual depth. SEM images for the groove in the scratch middle region (at an applied load of 200 mN) are also shown for the reference Ti sample and the $300\ \mathrm{mA/cm^2}$ sample

(which is similar to the 150 mA/cm^2 sample). The reference Ti sample presented a penetration depth of 2 μm under the maximum applied load (400 mN), and elastic recovery after loading release of 34%. The deformation mode was typically ductile, with progressive increase of the groove depth and with material piling up at the borders. The inner scars are due to third-body interaction with abraded and compacted material. On the other hand, the anodic layers presented a brittle behavior under scratching, with intense debris generation (Bhushan, 1999). Despite the large fluctuation, the elastic recovery was estimated as 33% for both anodized surfaces. However, the depths reached under maximum load were 4 μm (150 mA/cm^2) and 4.5 μm (300 mA/cm^2), surpassing the layer thicknesses (see Table 1) and exposing the Ti substrate beneath.

The deformation mechanism of the anodic layer can be better visualized in Fig. 7(b), which presents the complete scratch track for the 150 mA/cm^2 sample. The load increased linearly up to 400 mN during the scratch, from 120 to 720 μm. The insets (numbered as 1, 2, and 3) show regions with occurrence of cracks, debris release, and layer detachment due to the scratching. The plastic deformation and fracture become more severe from around the scratch distance 370 μm, which corresponds to 220 mN applied load. The penetration profile superimposed to the complete scratch image suggests that such an event coincides with the increase in the curve fluctuation, which is due, possibly, to the tip interaction with released fragments. This point can be assumed as the critical load for the layer strength under scratching, and the values for both anodic conditions are summarized in Table 1.

4.   Discussion

Kokubo and Takadama (2006) asserted that a material able to have apatite form on its surface in SBF has apatite produced on its surface in the living body, and bonds to living bone through this apatite layer; this phenomenon was verified by *in vivo* tests by Nishiguchi et al. (1999, 2001). Moreover, according to Kokubo and Takadama (2006), the ability level to form apatite on the surface of a material in SBF can predict the degree of *in vivo* bone bioactivity. According to these statements, since the HA was formed in SBF solution for both current densities used (Figs. 1(b), 2(d)–(e)), the titania layers produced by anodic oxidation using Ca–P-based electrolytes presented good bioactivity degree.

The layers' bioactivity can be attributed to a set of textural, structural, and chemical features. These aspects can be related to the titania layers produced in this work as follows.

(i) *Surface texture*. The layers' porosity (Fig. 2) and roughness (Table 1) have been reported as conditions affecting the cells attachment, differentiation, and proliferation, and avoiding micromotion of the prosthesis at the implant site (Braceras et al., 2007; Li et al., 2004; Liu et al., 2004; Zhu et al., 2001). Concerning the hydroxyapatite nucleation in SBF, and despite the differences in roughness and porosity depending on the choice of current density, no differences were observed between the samples prepared by the different treatment conditions. Actually, the role of pore size and roughness in the osseointegration process is not yet clear. It is reported that a porous structure and pore sizes ranging from 100 to 400 μm enhance bone ingrowth (Korkusuz and Korkusuz, 2004). On the other hand, Zhu et al. (2001) produced anodic layers using calcium glycerophosphate and calcium acetate with pore size of around 2 μm and roughness in the range of 0.8–0.98 μm which showed a high level of cell attachment. Likewise, Yu et al. (2007) obtained anodic layers containing Ca and P on Ti–6Al–4V presenting pore diameters in the order of 3 μm, with a fine connectivity between them; such features were considered by the authors to promote a strong bonding of the implant with living tissues. After all, considering the aforementioned studies, it is possible to assume that the porous structures obtained in the present work (with pore diameters 1–3 μm) are favorable to implant bioactivity, since the pores contribute to the anchorage of HA nuclei preceding the layer growing.

(ii) *Structural features*. Liu et al. (2004) and Yang et al. (2004) suggested that the TiO$_2$ phases rutile and anatase, identified by XRD in Fig. 1(a), are favorable substrates for HA nucleation. Notably, the arrangement of oxygen atoms in the rutile could, for certain atomic planes, match that of the HA planes (Yang et al., 2004). Following this line of thought, calcium phosphate integrating into the anodic layer, as identified by XRD, EDS and XPS, may present some structural affinity with HA. In studies conducted by Fini et al. (1999), Liu et al. (2005) and Yu et al. (2007), the Ca- and P-containing anodic layer is submitted to hydrothermal treatments, changing the calcium phosphate into a compound similar to HA. According to these authors, the titania plus HA layers can work similarly to HA coatings deposited on Ti, allowing a rapid formation of new bone on their surfaces.

(iii) *Chemical features*. The chemical nature of the layers can favor the growth of HA by surface charging and ion release in SBF. Noticeably, the anodic oxidation promoted an important increase in the hydroxyl amount at the Ti near surface, as identified by XPS (Fig. 3). Some authors (Chen et al., 2006; Lee et al., 2006; Simka et al., 2009) suggest that the dissociation of hydroxyl groups from the titania surface in the body fluid environment triggers the primary stage of HA nucleation. Phosphate ions from the body fluid are adsorbed on the charged surface, with subsequent adsorption of calcium ions on the phosphate ones. The relationship between the hydroxyl groups at the surface and bioactivity has also been proposed for other different treatments on Ti, such as calcium (Hanawa, 1999) and hydrogen (Xie et al., 2005) ionic implantations. Actually, the role of such chemical groups for HA nucleation on an artificial material soaked in SBF is well known in the literature (Kokubo et al., 2003; Takadama et al., 2001). Another possible contribution to the bioactivity in Ca-containing Ti surfaces is calcium release from the anodic layer to the body fluid, as suggested by Chen et al. (2006). The same was proposed by Hanawa (1999) for Ca-implanted Ti surfaces. According to these authors, the additional Ca^{2+} at the surface surroundings raises the local pH, which favors HA nucleation.

The elastic modulus and hardness of layers, as can be seen in Figs. 5, 6 and Table 1, presented no significant statistical differences with respect to the two current densities applied (150 and 300 mA/cm^2). Thus, the considerations about elastic modulus and hardness are relative to both current densities.

As previously mentioned, the elastic modulus of the implant biomaterial must be as close as possible to the bone tissue value in order to favor the transfer of functional loads between them (Liu et al., 2004; Mändl and Rauschenbach, 2002). As a consequence, stress shielding at the implant site is prevented, enhancing the stimulation of new bone growth and contributing to the quality and lifetime of the prosthesis (Niinomi, 2003, 2008; Niinomi et al., 2004). Obviously such interactions are critical at the interface between artificial material and living tissues. Based on these statements, the results show that the anodization process used provides an important improvement in the surface mechanical compatibility between metal and bone. The layers' elastic moduli were around ∼40 GPa, whereas the elastic modulus determined for bone tissues ranges from 10 to 40 GPa (Liu et al., 2004). Moreover, the elastic modulus of these Ca–P-based layers is still smaller than that of layers produced using different oxidation parameters. Using H$_2$SO$_4$ electrolytes, layers present an elastic modulus of ∼130 GPa (Santos Jr. et al., 2007), and using H$_3$PO$_4$, ∼120 GPa (Soares et al., 2008). In a previous work (de Souza et al., 2009) it is suggested that soft calcium phosphate agglomerates produced inside the layer during anodization can contribute to the overall low elastic modulus values.

The analytical method employed to calculate the actual layer hardness by correcting the effects of substrate gave consistent expected values. The empirical limit for the plastic deformation field produced by indentation being restrained inside the layer is 1/10 of the layer thickness (Fischer-Cripps, 2004; Saha and Nix, 2002); the calculated profiles for the 300 mA/cm^2 sample, presented in Fig. 6(b), follow those of the composite layer plus substrate up to about this limit. From the near surface region, the Ca–P-based layers presented hardness similar to that of metallic Ti, which, at first analysis, also corroborates to the mechanical compatibility of the implant surface with bone tissues. However, as observed by SEM (Fig. 4), there is a severe cracking around indentation imprints, indicating surface brittleness under the applied normal loads (up to 300 mN). Despite the increase in thickness with current density (Table 1), there was cracking occurring similarly in both conditions. The decrease of indentation hardness profiles for increasing loads (Fig. 6) is due to crack generation caused by the surface brittleness. Mikowski et al. (2007) suggested that, in brittle materials, the indentation hardness does not correspond to the response of the material plastic deformation, but the strength to the tip displacement due to fracture propagation. Therefore, the layers' indentation hardness in Fig. 6 is higher than the substrate hardness for low applied loads, but as the load increases the hardness decreases because the layer cracking allows higher penetration depths. Santos Jr. et al. (2007) and Soares et al. (2008) also reported hardnesses of anodic layers (produced with H$_2$SO$_4$ and H$_3$PO$_4$ electrolytes, respectively) that were higher than that of the Ti substrate, however with the effect of brittleness on the profiles less evidenced. The

elastic modulus is related to elastic interactions between atoms and molecules; but the elastic modulus measured by indentation methods is affected by cracking since it depends on the indentation contact area A_c, which is linearly dependent on the square of the contact depth h_c (Oliver and Pharr, 2004). However such an effect on elastic modulus is less intense than on the hardness, as can be seen in Fig. 5, due to the fact that it is proportional to $1/A^{1/2}$, whereas for the hardness it is proportional to $1/A$.

The brittleness of the Ca- and P-containing titania layers is even more evidenced in the scratch tests, shown in Fig. 7. Liu et al. (2004) asserted that oxide coatings synthesized by anodization in the dielectric rupture regime have high hardness, adhesion, strength, and wear resistance. Indeed, the coatings produced here presented superior tribological performance than that from alkaline heat treatment (AHT) (de Souza et al., 2010b), which is a well-known effective method to promote bioactivity on Ti surfaces (Kokubo et al., 2003; Nishiguchi et al., 1999, 2001; Takadama et al., 2001). In the AHT, the critical load for scratch tests was determined as 5.5 mN, whereas for these Ca–P anodic layers it was 220–280 mN. However, the anodic layers also presented a typical brittle behavior (Bhushan, 1999), quite distinct from that of the Ti substrate. Coating detachment by cracking and debris release in the scratch tests were observed, which are undesirable features for a biomaterial coating (Korkusuz and Korkusuz, 2004). Similar treatments on Ti were studied by Chen et al. (2006), using the same electrolyte and similar oxidation parameters, but the authors did not report any surface embrittlement. Notwithstanding, Zhu et al. (2001) accomplished a systematic study of layer growth and characterization, and suggested that an optimal combination of parameters can lead to high-quality coatings without microcracks, adhesive to the underlying substrate and showing positive biological response. Therefore, the tribological performance of the Ca- and P-containing layer can possibly be improved by the adjustment of parameters such as current density, final voltage, time, and electrolyte concentration.

5.   Conclusions

Titania anodic layers were produced on commercially pure Ti under galvanostatic mode using Ca–P-based electrolytes, using current densities (J) of 150 and 300 mA/cm^2. Layers presented Ca and P in their composition constituting a calcium phosphate compound, and the TiO$_2$ crystalline phases rutile and anatase. The rutile phase as well as layer porosity and roughness increased with current density. The layers presented good bioactivity in *in vitro* assays using SBF solution, which can be attributed to the combined effect of microstructure, layer porosity and hydroxyl radicals in plenty at the near surface. The elastic modulus and hardness of sample surfaces were evaluated by the instrumented indentation technique. Analytical methods were employed to obtain these properties for the anodic layers, subtracting the substrate effects. The elastic moduli of layers were about 40 GPa for both current densities, which are similar to the values for human bones (10–40 GPa). However, the anodic

layers presented brittleness under normal and tangential loading. The hardness decreased with indentation load due to cracking, varying from 5 GPa at the near surface to 1 GPa at depths equal to the layer thicknesses. The scratch tests performed with a Berkovich tip indicate that the layers undergo detachment from the substrate with loads 220 mN ($J = 150$ mA/cm^2) and 280 mN ($J = 300$ mA/cm^2).

Acknowledgements

REFERENCES

Battistoni, C., Casaletto, M.P., Ingo, G.M., Kaciulis, S., Mattogno, G., Pandolfi, L., 2000. Surface characterization of biocompatible hydroxyapatite coatings. Surf. Interface Anal. 29, 773–781.

Bertóti, I., Mohai, M., Sullivan, J.L., Saied, S.O., 1995. Surface characterization of plasma-nitrided titanium: an XPS study. Appl. Surf. Sci. 84, 357–371.

Bhattacharya, A.K., Nix, W.D., 1988. Analysis of elastic and plastic deformation associated with indentation testing of thin-films on substrates. Internat. J. Solids Structures 24, 1287–1298.

Bhushan, B., 1999. Nanomechanical properties of solid surfaces and thin films. In: Bhushan, B. (Ed.), Handbook of Micro/Nano Tribology. CRC Press LLC, Boca Raton.

Bhushan, B., 2001. Surface roughness analysis and measurement techniques. In: Bhushan, B. (Ed.), Modern Tribology Handbook, Volume One: Principles of Tribology. CRC Press LLC, Boca Raton.

Braceras, I., Alava, J.I., Goiketxea, L., de Maeztu, M.A., Onate, J.I., 2007. Interaction of engineered surfaces with the living world: ion implantation vs. osseointegration. Surf. Coat. Technol. 201, 8091–8098.

Chen, J., Shi, Y., Wang, L., Yan, F., Zhang, F., 2006. Preparation and properties of hydroxyapatite-containing titania coating by micro-arc-oxidation. Mater. Lett. 60, 2538–2543.

Chu, P.K., Chen, J.Y., Wang, L.P., Huang, N., 2002. Plasma-surface modification of biomaterials. Mat. Sci. Eng. R 36, 143–206.

Combes, C., Rey, C., Freche, M., 1998. XPS and IR study of dicalcium phosphate dihydrate nucleation on titanium surface. Colloids. Surf. B 11, 15–27.

de Jonge, L.T., Leeuwenburgh, S.C.G., Wolke, J.G.C., Jansen, J.A., 2008. Organic–inorganic surface modifications for titanium implant surfaces. Pharm. Res. 25, 2357–2369.

de Sena, L.A., Rocha, N.C.C., Andrade, M.C., Soares, G.A., 2003. Bioactivity assessment of titanium sheets electrochemically coated with thick oxide film. Surf. Coat. Technol. 166, 254–258.

de Souza, G.B., Foerster, C.E., da Silva, S.L.R., Lepienski, C.M., 2006. Nanomechanical properties of rough surfaces. Mater. Res. 9, 159–163.

de Souza, G.B., Lima, G.G., Kuromoto, N.K., Soares, P., Marino, C.E.B., Lepienski, C.M., 2009. Elastic modulus and hardness of bioactive Ti obtained by anodic oxidation using Ca/P-based solutions. Key Eng. Mater. 396–398, 323–326.

de Souza, G.B., Mikowski, A., Lepienski, C.M., Foerster, C.E., 2010a. Indentation hardness of rough surfaces produced by plasma-based ion implantation processes. Surf. Coat. Technol. 204, 3013–3017.

de Souza, G.B., Lepienski, C.M., Foerster, C.E., Kuromoto, N.K., Soares, P., Ponte, H.A., 2010b. Nanomechanical and nanotribological properties of bioactive titanium surfaces prepared by alkali treatment. J. Mech. Behav. Biomed. Mater. doi:10.1016/j.jmbbm.2010.07.005.

Fini, M., Cigada, A., Rondelli, G., Chiesa, R., Giardino, R., Giavaresi, G., Aldini, N.N., Torricelli, P., Vicentini, B., 1999. In vitro and in vivo behaviour of Ca- and P-enriched anodized titanium. Biomaterials 20, 1587–1594.

Fischer-Cripps, A.C., 2004. Nanoindentation. Springer-Verlag, New York.

FIZ Karlsruhe GmbH, 2008. Inorganic crystal structure database (ICSD, version 1.4.5, 2008-2). The National Institute of Standards & Technology, Karlsruhe.

Frauchiger, V.M., Schlottig, F., Gasser, B., Textor, M., 2004. Anodic plasma-chemical treatment of CP titanium surfaces for biomedical applications. Biomaterials 25, 593–606.

Gao, H., Chiu, C.-H., Lee, J., 1992. Elastic contact versus indentation modeling of multi-layered materials. Internat. J. Solids Structures 29, 2471–2492.

Hanawa, T., 1999. In vivo metallic biomaterials and surface modification. Mater. Sci. Eng. A 267, 260–266.

Hanawa, T., 2004. Metal ion release from metal implants. Mater. Sci. Eng. C 24, 745–752.

Kokubo, T., Kim, H.M., Kawashita, M., 2003. Novel bioactive materials with different mechanical properties. Biomaterials 24, 2161–2175.

Kokubo, T., Takadama, H., 2006. How useful is SBF in predicting in vivo bone bioactivity? Biomaterials 27, 2907–2915.

Korkusuz, P., Korkusuz, F., 2004. Hard tissue–biomaterial interactions. In: Yaszemski, M.J., et al. (Eds.), Biomaterials in Orthopedics. Marcel Dekker, New York, pp. 1–40.

Kunze, J., Muller, L., Macak, J.M., Greil, P., Schmuki, P., Muller, F.A., 2008. Time-dependent growth of biomimetic apatite on anodic TiO2 nanotubes. Electrochim. Acta 53, 6995–7003.

Kuromoto, N.K., Simão, R.A., Soares, G.A., 2007. Titanium oxide films produced on commercially pure titanium by anodic oxidation with different voltages. Mater. Charact. 58, 114–121.

Lee, J.-H., Kim, S.-E., Kim, Y.-J., Chi, C.-S., Oh, H.-J., 2006. Effects of microstructure of anodic titania on the formation of bioactive compounds. Mater. Chem. Phys. 98, 39–43.

Li, L.-H., Kong, Y.-M., Kim, H.-W., Kim, Y.-W., Kim, H.-E., Heo, S.-J., Koak, J.-Y., 2004. Improved biological performance of Ti implants due to surface modification by micro-arc oxidation. Biomaterials 25, 2867–2875.

Liu, X., Chu, P.K., Ding, C., 2004. Surface modification of titanium, titanium alloys, and related materials for biomedical applications. Mater. Sci. Eng. R 47, 49–121.

Liu, F., Song, Y., Wang, F., Shimizu, T., Igarashi, K., Zhao, L., 2005. Formation characterization of hydroxyapatite on titanium by microarc oxidation and hydrothermal treatment. J. Biosci. Bioeng. 100, 100–104.

Lu, G., Bernasek, S.L., Schwartz, J., 2000. Oxidation of a polycrystalline titanium surface by oxygen and water. Surf. Sci. 458, 80–90.

Mändl, S., Rauschenbach, B., 2002. Improving the biocompatibility of medical implants with plasma immersion ion implantation. Surf. Coat. Technol. 156, 276–283.

Mikowski, A., Soares, P., Wypych, F., Gardolinski, J.E.F.C., Lepienski, C.M., 2007. Mechanical properties of kaolinite macro-crystals. Phil. Mag. 87, 4445–4459.

Milman, Y.V., Chugunova, S.I., 1999. Mechanical properties, indentation and dynamic yield stress of ceramic targets. Int. J. Impact Eng. 23, 629–638.

Moulder, J.F., Stickle, W.F., Sobol, P.E., Bomben, K.D., 1992. Handbook of X-ray Photoelectron Spectroscopy. Perkin-Elmer Corp., Eden Prairie, MN.

Niinomi, M., 2003. Fatigue performance and cyto-toxicity of low rigidity titanium alloy, Ti-29Nb-13Ta-4.6Zr. Biomaterials 24, 2673–2683.

Niinomi, M., 2008. Mechanical biocompatibilities of titanium alloys for biomedical applications. J. Mech. Behav. Biomed. Mater. 1, 30–42.

Niinomi, M., Hattori, T., Niwa, S., 2004. Material characteristics and biocompatibility of low rigidity titanium alloys for biomedical applications. In: Yaszemski, M.J., et al. (Eds.), Biomaterials in Orthopedics. Marcel Dekker, New York, pp. 41–62.

Nishiguchi, S., Nakamura, T., Kobayashi, M., Kim, H.M., Miyaji, F., Kokubo, T., 1999. The effect of heat treatment on bone-bonding ability of alkali-treated titanium. Biomaterials 20, 491–500.

Nishiguchi, S., Kato, H., Fujita, H., Oka, M., Kim, H.M., Kokubo, T., Nakamura, T., 2001. Titanium metals form direct bonding to bone after alkali and heat treatments. Biomaterials 22, 2525–2533.

NIST—National Institute of Standards and Technology, 2010. X-ray photoelectron spectroscopy database, USA. Available in: http://srdata.nist.gov/xps/.

Oliver, W.C., Pharr, G.M., 2004. Measurement of hardness and elastic modulus by instrumented indentation: advances in understanding and refinements to methodology. J. Mater. Res. 19, 3–20.

Paital, S.R., Dahotre, N.B., 2009. Calcium phosphate coatings for bio-implant applications: materials, performance factors, and methodologies. Mater. Sci. Eng. R 66, 1–70.

Saha, R., Nix, W.D., 2002. Effects of the substrate on the determination of thin film mechanical properties by nanoindentation. Acta Mater. 50, 23–38.

Santos Jr., E., Kuromoto, N.K., Soares, G.A., 2007. Mechanical properties of titania films used as biomaterials. Mater. Chem. Phys. 102, 92–97.

Simka, W., Iwaniak, A., Nawrat, G., Maciej, A., Michalska, J., Radwanski, K., Gazdowicz, J., 2009. Modification of titanium oxide layer by calcium and phosphorus. Electrochim. Acta 54, 6983–6988.

Soares, P., Mikowski, A., Lepienski, C.M., Santos Jr., E., Soares, G.A., Swinka Filho, V., Kuromoto, N.K., 2008. Hardness and elastic modulus of TiO_2 anodic films measured by instrumented indentation. J. Biomed. Mater. Res. B 84, 524–530.

Sul, Y.T., Johansson, C.B., Petronis, S., Krozer, A., Jeong, Y., Wennerberg, A., Albrektsson, T., 2002. Characteristics of the surface oxides on turned and electrochemically oxidized pure titanium implants up to dielectric breakdown: the oxide thickness, micropore configurations, surface roughness, crystal structure and chemical composition. Biomaterials 23, 491–501.

Takadama, H., Kim, H.-M., Kokubo, T., Nakamura, T., 2001. XPS study of the process of apatite formation on bioactive Ti–6Al–4V alloy in simulated body fluid. Sci. Tech. Adv. Mater. 2, 389–396.

Wojdyr, M., 2010. Fityk 0.9.1, 2001–2010. Warsaw, Poland. Available in: http://www.unipress.waw.pl/fityk/.

Xie, Y., Liu, X., Huang, A., Ding, C., Chu, P.K., 2005. Improvement of surface bioactivity on titanium by water and hydrogen plasma immersion ion implantation. Biomaterials 26, 6129–6135.

Xu, H., Pharr, G.M., 2006. An improved relation for the effective elastic compliance of a film/substrate system during indentation by a flat cylindrical punch. Scr. Mater. 55, 315–318.

Yang, B., Uchida, M., Kim, H.-M., Zhang, X., Kokubo, T., 2004. Preparation of bioactive titanium metal via anodic oxidation treatment. Biomaterials 25, 1003–1010.

Yen, S.K., 1999. Retardation effects of thermally grown oxide films on the hydrogen embrittlement of commercial pure titanium. Corros. Sci. 41, 2031–2051.

Yu, S.R., Yang, X.Z., Yang, L., Liu, Y.H., Yu, Y.J., 2007. Novel technique for preparing Ca- and P-containing ceramic coating on Ti–6Al–4V by micro-arc oxidation. J. Biomed. Mater. Res. B 83, 623–627.

Zhu, X., Kim, K.H., Jeong, Y., 2001. Anodic oxide films containing Ca and P of titanium biomaterial. Biomaterials 22, 2199–2206.